J Mater Sci (2010) 45:6521–6527
DOI 10.1007/s10853-010-4741-8

Sintering of a fine-grained $BaCeO_3$ powder obtained from a co-precipitation method

Roberto Köferstein · Lothar Jäger · Stefan G. Ebbinghaus

Received: 28 May 2010 / Accepted: 25 June 2010 / Published online: 7 July 2010
© Springer Science+Business Media, LLC 2010

Abstract The formation of $BaCeO_3$ by a co-precipitation method is described herein. The co-precipitation route leads to an orange (BaCe)-precursor powder (**1**). To improve the sintering behaviour, a small amount of Ge^{4+} was incorporated, leading to a ($BaCe_{0.95}$/$Ge_{0.05}$)-precursor (**2**). Both precursor powders results in fine-grained preceramic powders (**1A**, **2A**) after calcination. The shrinkage and sintering behaviour of resulting powder compacts were studied in comparison to a coarse-grained mixed-oxide $BaCeO_3$ powder (**3**). Compacts of **2A** reach a relative density of 90% after sintering at 1350 °C with grain sizes between 0.9 and 3.2 μm. On the other hand ceramics of **1A** and **3** have, after sintering at 1500 °C (10 h), relative densities of 85 and 76%, respectively. Ceramic bodies of **1A** consisted of phase-pure orthorhombic $BaCeO_3$, whereas bodies of **2A** show reflections of $BaCeO_3$ and a Ba_2GeO_4 phase. DTA investigations of samples **1A** and **2A** reveal three phase transitions at 255 °C (**1A**) and 256 °C (**2A**) as well as 383 °C (**1A**) and 380 °C (**2A**). A very weak one can be obtained in the range 880–910 °C.

Introduction

Perovskite materials based on $BaCeO_3$ have high proton conductivity in hydrogen and water containing atmospheres between 600 and 800 °C. Therefore, $BaCeO_3$-based compounds are candidates to replace yttria-stabilized zirconia (YSZ) electrolyte materials for solid oxide fuel cells (SOFCs) [1–9]. Benlhachemi et al. [10] and Popescu et al. [11] reported on the catalytic oxidation of methane in the presence of $BaCeO_3$. Furthermore, barium cerate can be also applied as a functional material for semiconductor gas sensors [12] and solid solution of the type $BaTi_{1-x}Ce_xO_3$ can be used for capacitor applications [13–18]. High-resolution neutron diffraction measurements up to 1000 °C by Knight [19, 20] and Genet et al. [21] evidence three phase transitions of $BaCeO_3$. A first transition at 290 °C leads from a primitive orthorhombic perovskite structure (Space group: *Pmcn*) to the body-centred one (*Incn*), a second at 400 °C to a rhombohedrally distorted one ($F\,\bar{3}2$) and the last transition at 900 °C to the cubic perovskite structure ($Pm\,\bar{3}m$).

Compacts on the basis of $BaCeO_3$ generally reveal only a moderate densification behaviour. For application such as capacitors or in SOFCs the density of the sintering bodies must be high [22–30]. On the other hand, sintering temperatures above 1500 °C should be avoided because $BaCeO_3$ melts incongruently at 1480 ± 5 °C with the formation of CeO_2 and a liquid containing BaO [6, 31]. The densification behaviour can be improved and thus the sintering temperature reduced by using fine-grained powders and sintering additives [32–34]. Apart from the mixed-oxide method, which results in coarse-grained powders, some wet chemical syntheses have been developed to obtain fine-grained $BaCeO_3$ powders such as various precursor complex methods, solvothermal and sol–gel syntheses [28, 35–40]. Pechini-based routes are reported by Lee et al. [41] and Su et al. [42]. Almost all of those preparation methods use as starting materials Ce^{3+} compounds to obtain $BaCeO_3$. On the other hand, it seem to be advantageous to use Ce^{4+} compounds as starting

R. Köferstein (✉) · L. Jäger · S. G. Ebbinghaus
Institut für Chemie, Anorganische Chemie, Martin-Luther-Universität Halle-Wittenberg, Kurt-Mothes Strasse 2, 06120 Halle, Germany
e-mail: roberto_koeferstein@web.de

material to synthesize $BaTi_{1-x}Ce_xO_3$ solid solutions by wet chemical methods [43].

In this paper we therefore describe a simple co-precipitation method starting from a Ce^{4+} compound to obtain fine-grained $BaCeO_3$. Additionally, we have studied the phase evolution during the decomposition process. The sintering behaviour of $BaCeO_3$ compacts, the microstructure of the resulting ceramic bodies, and the influence of a sintering additive have been also investigated. Phase transition temperatures have been determined by DTA measurements.

Experimental

Material preparation

$Ba(NO_3)_2$ (0.04 mol, Merck) and $(NH_4)_2Ce(NO_3)_6$ (0.04 mol, Alfa Aesar) were separately dissolved in 50 mL water. Both solutions were combined in a round bottom flask cooled with ice. Under vigorous stirring ammonium oxalate solution (0.16 mol in 440 mL water) and afterwards a cooled mixture (5 °C) of 66 mL concentrated ammonia solution (25%), 33 mL hydrogen peroxide solution (30%) and 50 mL water were added starting an exothermic reaction to form an orange precipitate. The mixture was stirred in an ice bath for 30 min, filtered and the precipitate was washed with water several times. The resulting orange product (**1**) was dried in air for 1 day and then dried over H_2SO_4 in a desiccator for 7 days.

Precursor **2** was synthesized analogously to precursor **1**. However, 5 mol% of $(NH_4)_2Ce(NO_3)_6$ was substituted by $Ge(OC_2H_5)_4$.

For the shrinkage and sintering studies the precursors **1** and **2** were calcined in static air at 980 °C by a heating rate controlled thermal treatment to obtain fine-grained powders **1A** and **2A**, as described below. These calcined powders were milled with ZrO_2-balls in propan-2-ol for 2 h (m_{powder}:m_{balls} = 1:4). After filtering and drying, the powders were mixed with 5 mass% of a saturated aqueous solution of polyvinyl alcohol (PVA) as a pressing aid, then the powders were pressed to discs with a green density of about 2.7–2.8 g/cm^3.

For comparative purposes, $BaCeO_3$ powder (**3**) was also prepared via a conventional mixed-oxide method. Equivalent amounts of $BaCO_3$ (J.T. Baker Inc) and CeO_2 (Acros Organics) were milled for 24 h using ZrO_2-balls in water (m_{powder}:m_{balls}:m_{water} = 1:1:4). After filtering off and drying the mixture was calcined in static air (rate 10 K/min) for 4 h at 1150 °C. The remaining steps were identical to those mentioned above (as for **1A**). However, the green densities of the compacts were 3.5 g/cm^3.

Characterization

X-ray powder diffraction (XRD) patterns were recorded on a STOE STADI MP diffractometer at 25 °C using Co $K\alpha_1$ radiation. The powder patterns were indexed and refined with the software suite WinXPOW [44] using the TREOR method [45]. Fourier transform attenuated total reflection infrared (ATR-IR) spectra in the range 4000–400 cm^{-1} (resolution: 4 cm^{-1}) were obtained using a Tensor 27 FT-IR spectrometer from Bruker with an ATR unit (MVP 2 Series from Harrick). Dilatometric (shrinkage) investigations were performed in a flowing synthetic air atmosphere (50 mL/min) in a TMA 92-16.18 unit from Setaram. Thermogravimetric (TG) and differential thermoanalytic (DTA) measurements were achieved using a Netzsch STA 449 System (heating/cooling rate 10 K/min, flowing air or argon (30 mL/min)). For the investigation of phase transitions each DTA sample was measured three times to ensure reproducibility. The specific surface area was determined using nitrogen three-point BET (Nova 1000, Quantachrome Corporation). The equivalent BET particle diameter was calculated assuming the powder particles were spherical or cubic in shape [46]. Scanning electron microscope images were recorded with a Philips XL30 Environmental Scanning Electron Microscope (ESEM).

Results and discussion

Powder characterization

Figure 1 shows the IR spectrum of the orange (BaCe)-precursor **1**. A broad band round 3600–3000 cm^{-1} reveals OH stretching vibrations. Vibration maxima at 1601, 1310 and 1059 cm^{-1} represent HOH bending modes as well as the presence of oxalate anions [47–49]. The band at

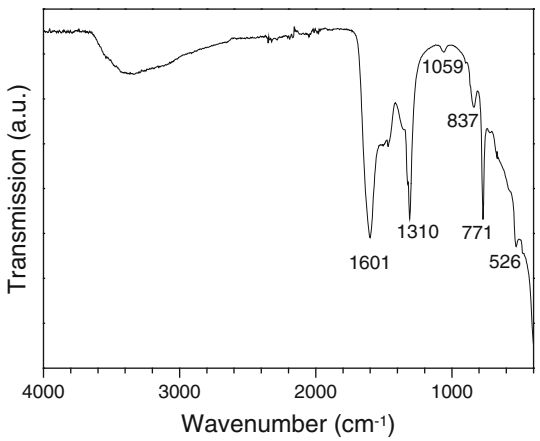

Fig. 1 IR spectrum of precursor **1**

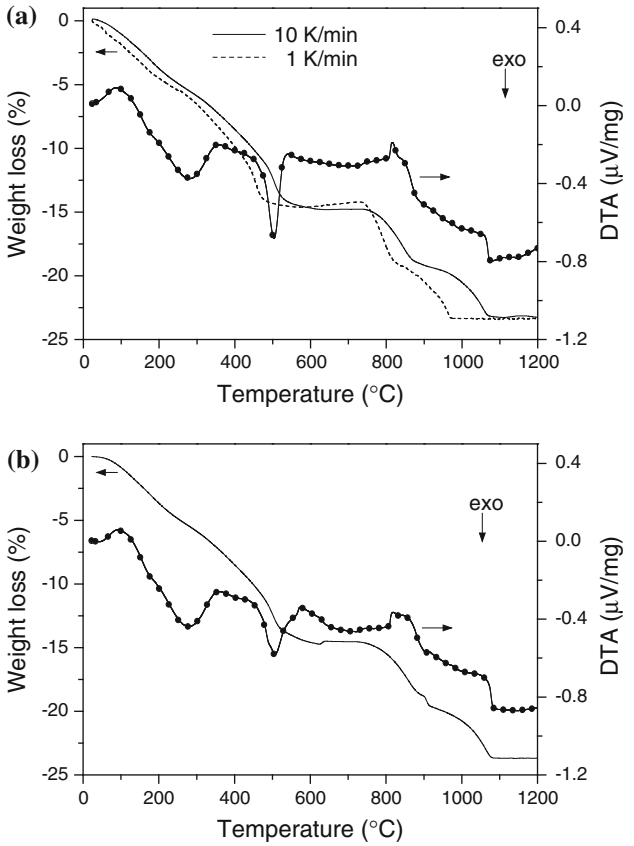

Fig. 2 TG and DTA curves of precursor **1** in different atmospheres. **a** Flowing air (DTA traces for a heating rate of 1 K/min not shown), **b** argon. Every 100th data point in the DTA curve is marked by a *symbol*

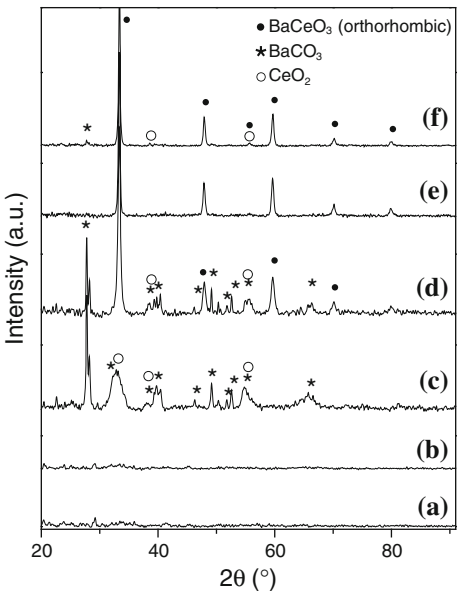

Fig. 3 XRD patterns (recorded at 25 °C) of precursor powder **1** (*a*) and decomposition products (*b–e*) of **1** at various temperatures (soaking time 1 h, rate 10 K/min): *b* 400 °C, *c* 600 °C, *d* 800 °C, *e* 1000 °C. *f* Powder **1A** from a heating rate controlled calcination process at 980 °C

837 cm^{-1} can be assigned to a peroxo group [47, 50–53]. Additionally, bands at 771 and 526 cm^{-1} can be observed.

TG and DTA investigations in flowing air and argon atmosphere are shown in Fig. 2. In flowing air (Fig. 2a) we observed a weight loss of 14.7% up to 600 °C, which is accompanied by two exothermic signals between 90–350 °C and 420–530 °C. This level is stable until 730 °C and consists of orthorhombic $BaCO_3$ and CeO_2 [59] (see also Fig. 3). A following two-step weight loss up to 1070 °C leads to the formation of $BaCeO_3$. During this process an endothermic peak with an onset temperature of 810 °C can be observed. This endothermic signal is mainly caused by the phase transition from orthorhombic to hexagonal $BaCO_3$ and its following decomposition [54–58]. The total weight loss is 23.3%. TG/DTA measurements in air with a heating rate of 1 K/min shows that up to 970 °C the (BaCe)-precursor is completely transformed into $BaCeO_3$. Thermoanalytic measurements in argon atmosphere reveal a very similar decomposition behaviour (Fig. 2b). The onset and offset temperatures of the DTA peaks do not significantly differ from air measurement. The decomposition is finished at 1080 °C and exhibits a total weight loss of 23.7%. XRD investigations of the final white product indicate orthorhombic $BaCeO_3$.

Phase evolution during the thermal decomposition of the amorphous (BaCe)-precursor **1** is shown in Fig. 3. The samples were heated in a muffle furnace in static air (rate 10 K/min). Calcination at 400 °C for 1 h results in a yellow X-ray amorphous powder (Fig. 3b). It can be seen in Fig. 3a and b in which the diffractograms show very weak peaks indicating a small crystalline amount into the powders. However, those weak peaks could not be assigned. Reflections of orthorhombic $BaCO_3$ and cubic CeO_2 [59] appear after heating at 600 °C (Fig. 3c). Heat treatment at 800 °C leads to a light-yellow powder consisting of $BaCO_3$, CeO_2 and $BaCeO_3$ [59] (Fig. 3d). At 900 °C the amount of $BaCeO_3$ increases and the colour of the resulting powder turns to white. The XRD pattern after calcination at 1000 °C reveals only reflections of orthorhombic $BaCeO_3$ (Fig. 3e).

Sintering behaviour and characterization of ceramic bodies

As seen in Fig. 2a the final temperature for the formation of $BaCeO_3$ depends on the heating rate. For the following investigations, therefore, the (BaCe)-precursor **1** was calcined by the following thermal treatment in static air: heating to 600 °C with a heating rate of 10 K/min, slow heating with 1 K/min to 980 °C, and subsequently cooling with 5 K/min to room temperature. The resulting white

$BaCeO_3$ powder (**1A**) has a specific surface area of $S = 5.8$ m^2/g and an equivalent particle size of 163 nm which can be considered as an average size of the primary particles [60]. As seen in Fig. 3f powder **1A** consists of a $BaCeO_3$ perovskite phase and a very small amount of $BaCO_3$ and CeO_2. The coarse-grained powder **3** resulting from a mixed-oxide process after calcinations at 1150 °C for 4 h has a specific surface area of 2.1 m^2/g and an equivalent particle size of 449 nm. To improve the sintering behaviour we additionally substituted 5 mol% of $(NH_4)_2Ce(NO_3)_6$ by $Ge(OC_2H_5)_4$ during the co-precipitation synthesis and obtained an amorphous $(BaCe_{0.95}/Ge_{0.05})$-precursor (**2**). Precursor **2** was calcined by the same thermal treatment as described for precursor **1** resulting in a white powder (**2A**).

Figure 4 shows the non-isothermal dilatometric investigations up to 1500 °C. Samples **1A** and **2A** begin to shrink at about 1010–1020 °C. Sample **1A** shows a defined shrinkage rate maximum at 1197 °C (rate: −0.5%/min) and a second broad maximum with a rate of −0.35%/min at 1329 °C. In contrast, sample **2A** shows a very broad change of the shrinkage rate. Maxima appear at 1204 °C (rate: −0.36%/min) and about 1386 °C (rate: −0.63%/min). The shrinkage of sample **3** starts at the significantly higher temperature of about 1230 °C and shows two maxima of the shrinkage rate at 1383 °C (rate: −0.22%/min) and at 1456 °C (rate: −0.33%/min), respectively. The shrinkage rates of all samples indicate that the densification is dominated by sliding processes. Diffusion as the dominant process causes only shrinkage rates of about 10^{-4} to 10^{-1}%/min [33, 61, 62].

The evolution of the bulk densities of ceramic bodies of **1A**, **2A** and **3** after isothermal sintering with a soaking time of 1 and 10 h is represented in Fig. 5. The bulk densities of the ceramic bodies were calculated from their weight and geometric dimensions. The relative densities of sample **1A** and **3** are related to the theoretical density (single crystal density) of 6.36 g/cm^3 [63] and the densities of sample **2A** are related to 6.29 g/cm^3 [64]. It can be seen that the relative densities of ceramic bodies of **3** remain always considerably below 80%. Ceramics from the co-precipitation method (**1A**) exhibit a relative density of 85% and grain sizes between about 2–12 μm after sintering for 10 h at 1500 °C (Fig. 5b, 6a). The addition of Ge^{4+} during the co-precipitation synthesis considerably improves the sintering behaviour of the resulting preceramic powder (**2A**). We obtained dense ceramic bodies (relative density ≥90%) after 1 h at 1500 °C and even at 1350 °C after 10 h sintering (Fig. 5a, b). After a soaking time of 10 h the

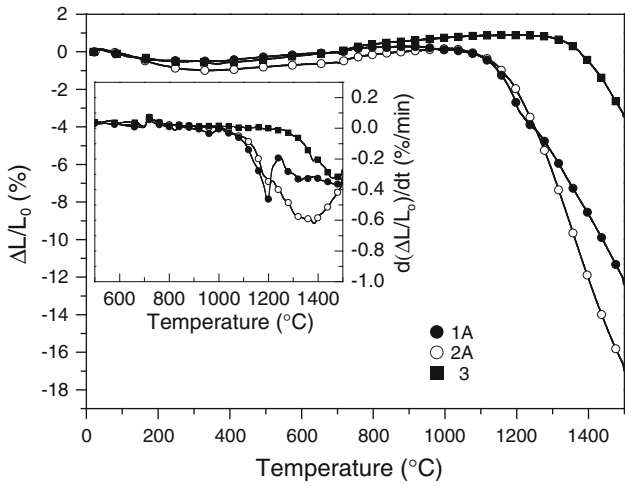

Fig. 4 Non-isothermal dilatometric measurements in flowing air of green bodies of **1A**, **2A** and **3** (heating rate 10 K/min). The *inset* shows the relative shrinkage rates ($d(\Delta L/L_0)/dt$). Every 100th data point is marked by a *symbol*

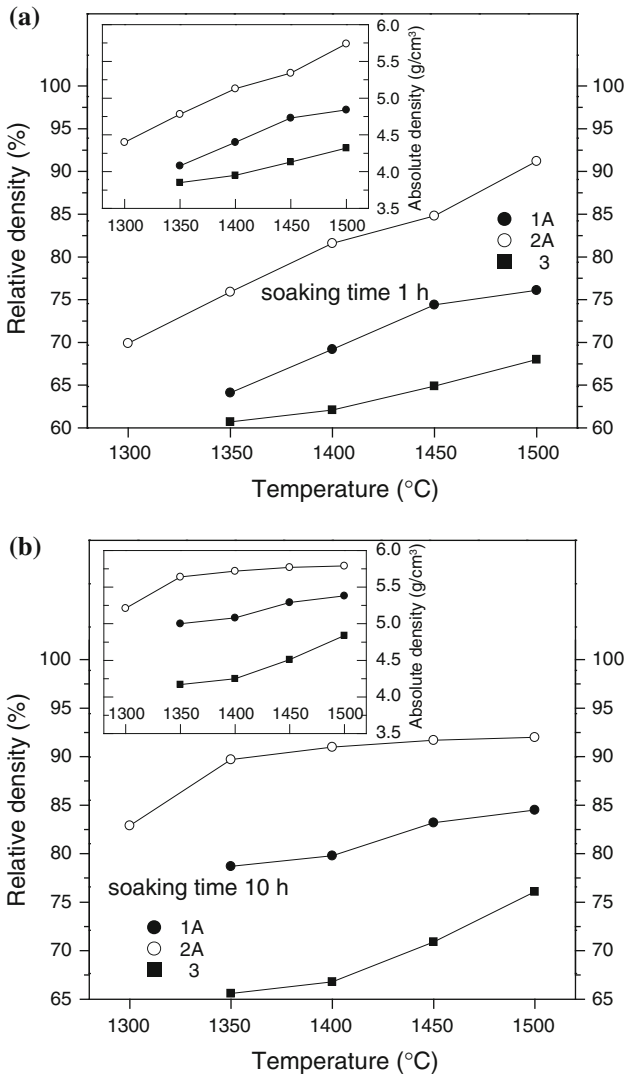

Fig. 5 Evolution of the final densities of ceramic bodies of **1A**, **2A** and **3** after an isothermal sintering process of **a** 1 h and **b** 10 h (rate 10 K/min)

microstructure shows grain sizes between 0.9 and 3.2 μm (1350 °C, Fig. 6b), 1–5 μm (1400 °C), 1.5–6.5 μm (1450 °C, Fig. 6c) and 2.5–12 μm (1500 °C, Fig. 6d). Sintering of **2A** at 1300 °C for 50 h results in ceramics with a relative density of 88% and grain sizes between about 0.8–2.2 μm (Fig. 6e). DTA investigations up to 1460 °C of sample **2A** do not show the formation of a liquid phase. Heat treatment below 1500 °C, therefore, is characterized by solid-state sintering. Hence, the addition of Ge^{4+} during the synthesis improves the densification process by supporting sliding processes [62, 65–67].

XRD patterns of ceramic bodies of **1A**, **2A** and **3** after sintering at 1400 °C for 1 h are shown in Fig. 7. Ceramics of **1A** and **3** show only reflections of orthorhombic $BaCeO_3$ [59] (Fig. 7a, b). XRD data of ceramic bodies (corrected by an internal standard) were indexed on the basis of a primitive orthorhombic unit cell (*Pmcn*) according to Knight et al. [19, 20, 63]. The cell parameters were determined by least-square refinements. For $BaCeO_3$ ceramic bodies of **1A** lattice parameters of $a = 877.56(14)$ pm, $b = 623.66(8)$ pm, $c = 621.52(14)$ pm, $V = 340.15(8)$ pm^3 were calculated. These parameters agree very well with earlier data for pure $BaCeO_3$ [19, 20, 63]. XRD investigations of ceramics of **2A** (Fig. 7c) show the pattern of orthorhombic $BaCeO_3$. Closer inspections in the range $2\theta = 33°–39°$ reveal reflections belonging to an orthorhombic Ba_2GeO_4 phase [59]. The appearance of Ba_2GeO_4 indicates the presence of CeO_2. In Fig. 7c a weak reflection

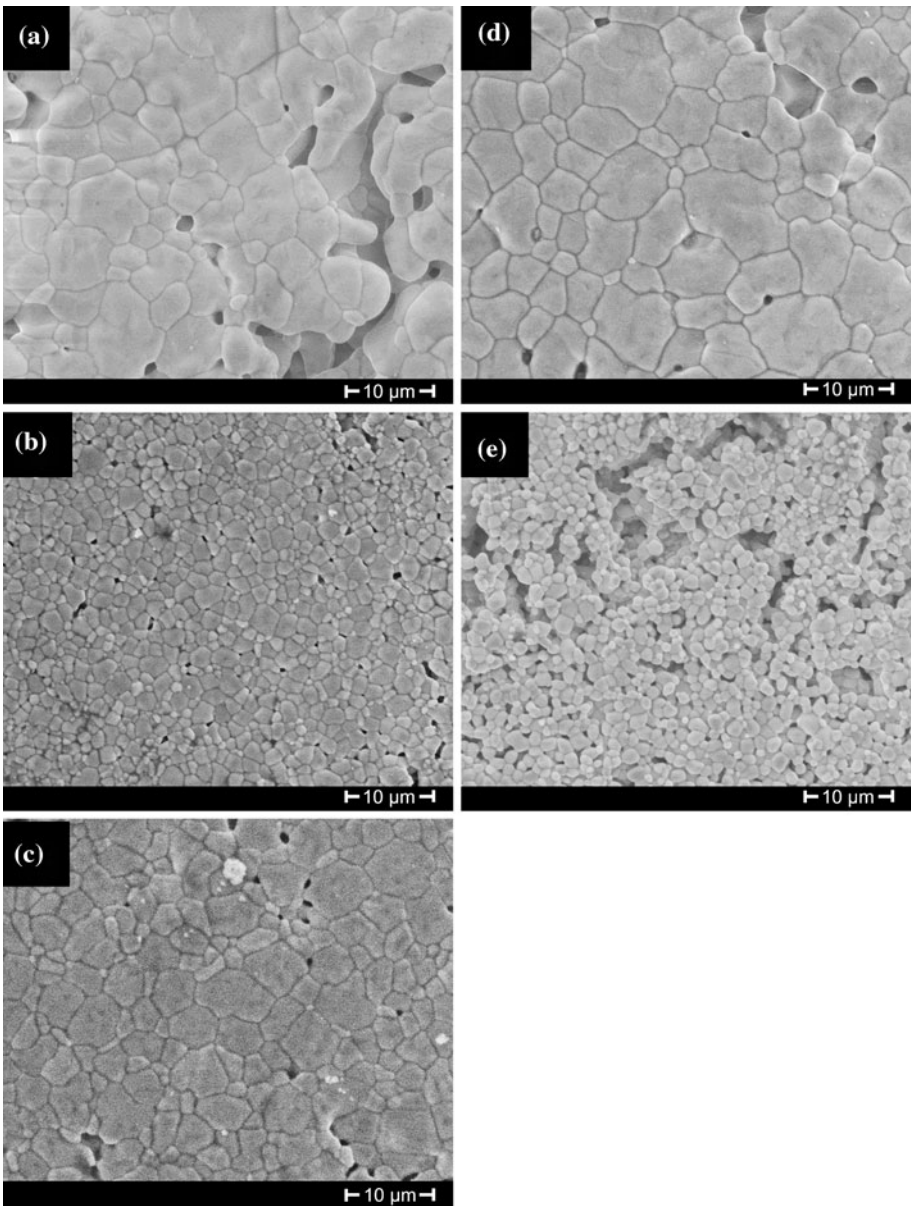

Fig. 6 SEM images of the surface of ceramic bodies after various sintering treatments (heating rate 10 K/min). Ceramic **1A**: **a** 1500 °C, 10 h. Ceramic **2A**: **b** 1350 °C, 10 h; **c** 1450 °C, 10 h; **d** 1500 °C, 10 h; **e** 1300 °C, 50 h

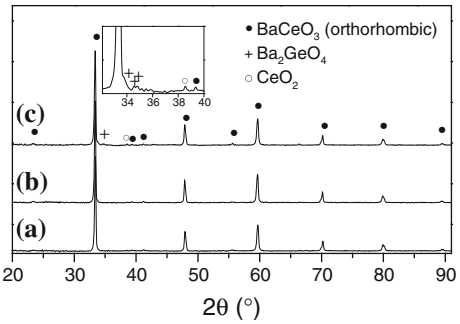

Fig. 7 XRD patterns (recorded at 25 °C) of ceramic bodies sintered at 1400 °C for 1 h. *a* Ceramic **3**, *b* ceramic **1A**, *c* ceramic **2A**

at $2\theta = 38.6°$ appeared representing the (200) reflection of cubic CeO_2. Lattice constants and therefore the unit cell volume of the $BaCeO_3$ phase of ceramics of **2A** do not significantly differ from the data of ceramics of **1A**. From this finding it can be concluded, that the addition of Ge^{4+} during the synthesis and the following calcinations and sintering procedure does not lead to an incorporation of Ge^{4+} into the $BaCeO_3$ lattice.

DTA data of ceramics of **1A**, **2A** and **3** are presented in Fig. 8. All samples show reversible endothermic effects between 250–280 °C, 370–400 °C (Fig. 8b), and a very weak one between 890 and 910 °C (Fig. 8c), representing three phase transitions, as mentioned above. The onset temperatures of the first two peaks could be determined. Sample **3** reveals onset temperatures at 260 and 387 °C. The onset temperatures of samples **1A** and **2A** are slightly shifted to lower temperatures of 255 and 383 °C (**1A**) as well as 256 and 380 °C (**2A**). The observed phase transition temperatures agree very well with earlier DSC and high temperature neutron diffraction studies [19, 68, 69].

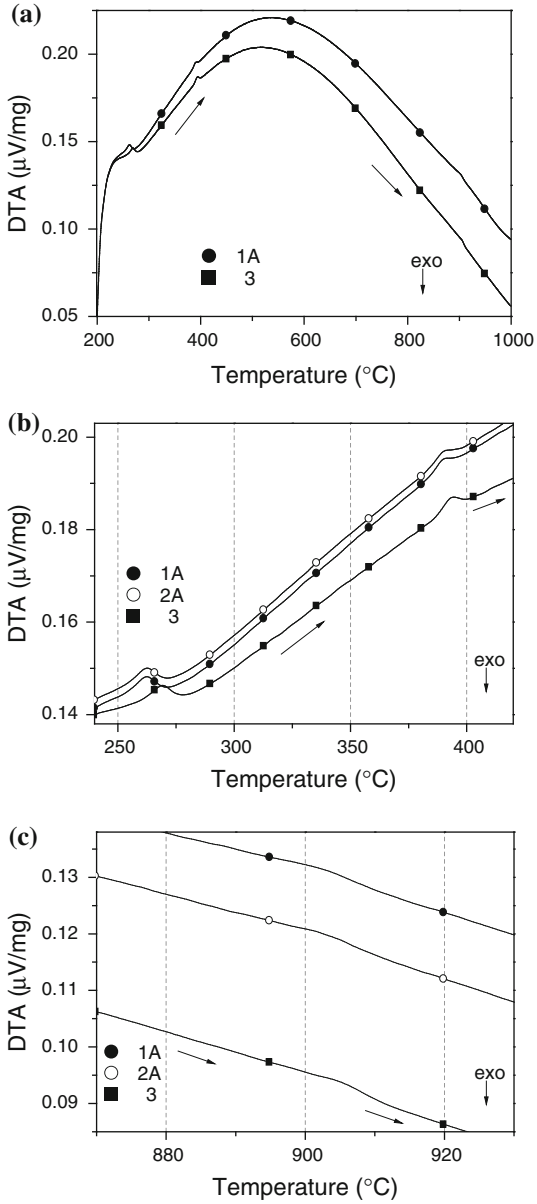

Fig. 8 DTA traces in flowing air of ceramic bodies of **1A**, **2A** and **3** sintered at 1400 °C for 1 h. Heating rate 10 K/min. **a** The whole DTA curves of ceramic **1A** and **3** (ceramic **2A** is not shown for clarity). **b** DTA curves of **1A**, **2A** and **3** between 240 and 420 °C. **c** DTA curves of **1A**, **2A** and **3** around 900 °C. Every 500th (**a**) and 100th (**b**, **c**) data point is marked by a *symbol*

Conclusion

Fine-grained $BaCeO_3$ powders can be prepared by a co-precipitation method using a Ce^{4+} salt. The temperature for the formation of $BaCeO_3$ depends on the heating rate, and is 970 °C with a heating rate of 1 K/min. A rate controlled calcination procedure of the X-ray amorphous (BaCe)-precursor powder (**1**) leads to a $BaCeO_3$ powder (**1A**) with a specific surface area of 5.8 m^2/g. $BaCeO_3$ powder (**3**) prepared by a mixed-oxide method has a specific surface area of 2.1 m^2/g and shows an insufficient sintering behaviour. On the other hand, sintering of compacts of **1A** to 1500 °C for 10 h leads to a bulk density of 85%. The sintering behaviour can be considerably improved using a sintering aid. During the co-precipitation synthesis 5 mol% of the Ce^{4+} salt were substituted by Ge^{4+}-alkoxide forming a $(BaCe_{0.95}/Ge_{0.05})$-precursor (**2**). Powder compacts of the resulting calcined powder **2A**, containing a Ba–Ge–O phase, reach a relative density of 90% with grain sizes between 0.9 and 3.2 µm after sintering at 1350 °C and a soaking time of 10 h. The Ba–Ge–O phase improves the densification process by supporting sliding processes and do not act as a liquid phase former. The final ceramics of **1A** and **3** consist of phase-pure orthorhombic $BaCeO_3$. XRD patterns of ceramics of **2A** shows small reflections of Ba_2GeO_4 and CeO_2 besides the reflections of $BaCeO_3$.

DTA measurements up to 1000 °C of ceramics of **1A**, **2A** and **3** reveal three reversible phase transitions.

Acknowledgements The authors thank Dr. Th. Müller for dilatometric and TG/DTA measurements. Financial support by the Federal State Saxony-Anhalt (Cluster of Excellence "Nanostructured Materials") is gratefully acknowledged.

References

1. Tao Z, Zhu Z, Wang H, Liu W (2010) J Power Sources 195:3481
2. Künstler K, Lang H-J, Maiwald A, Tomandl G (1998) Solid State Ionics 107:221
3. Scherban T, Lee W-K, Nowick AS (1988) Solid State Ionics 28–30:585
4. Katahira K, Kohchi Y, Shimura T, Iwahara H (2000) Solid State Ionics 138:91
5. Gorbova E, Maragou V, Medvedev D, Demin A, Tsiakaras P (2008) Solid State Ionics 179:887
6. Ryu KH, Haile SM (1999) Solid State Ionics 125:355
7. Iwahara H, Uchida H, Morimoto K (2000) J Electrochem Soc 137:462
8. Lva J, Wang L, Lei D, Guoa H, Kumar RV (2009) J Alloys Compd 467:376
9. Ma Q, Peng R, Lin Y, Gao J, Meng G (2006) J Power Sources 161:95
10. Benlhachemi A, Ouzaouit K, Benyaich H, Villain S, Gavarri JR (2008) Phys Chem News 41:50
11. Popescu I, Marcu I-C, Sandulescu I, Macovei D (2006) Prog Catal 15:79
12. Hibino T, Iwahara H (1993) Sens Actuators B13–14:483
13. Chen A, Zhi Y, Zhi J, Vilarinho PM, Baptista JL (1997) J Eur Ceram Soc 17:I2
14. Li ZC, Bergman B (2005) J Eur Ceram Soc 25:441
15. Komatsu K (1997) Barium titanium cerium oxide dielectric ceramic composition with high dielectric constant and small dielectric constant shift by temperature changes. JP Patent No. 09157011 A
16. Baxter P, Hellicar NJ, Lewis B (1959) J Am Ceram Soc 42:465
17. Kolar D, Guha JP, Buh M (1972) Proc Brit Ceram Soc 23:152
18. Lu D-Y, Sun X-Y, Toda M (2007) J Phys Chem Solids 68:650
19. Knight KS (1994) Solid State Ionics 74:109
20. Knight KS (2001) Solid State Ionics 145:275
21. Genet F, Loridant S, Ritter C, Lucazeau G (1999) J Phys Chem Solids 60:2009
22. Cernea M, Manea A, Piazza D, Galassi C, Vasile E (2007) J Am Ceram Soc 90:1728
23. Rice RW (1998) Porosity of ceramics. Marcel Dekker, New York, pp 325
24. Singh P, Parkash O, Kumar D (2005) Solid State Ionics 176:2167
25. He Z, Ma J, Zhang R (2004) Ceram Int 30:1353
26. Iddles DM, Bell AJ, Moulson AJ (1992) J Mater Sci 27:6303. doi:10.1007/BF00576276
27. Azad AM, Hon NC (1998) J Alloys Compd 270:95
28. Osman N, Talib IA, Hamid HA (2009) Ionics 15:203
29. Gorbova E, Maragou V, Medvedev D, Demin A, Tsiakaras P (2008) J Power Sources 181:292
30. Chen FL, Sorensen T, Meng GY, Peng DK (1998) J Eur Ceram Soc 18:1389
31. Guha JP, Kolar D (1971) J Mater Sci 6:1174. doi:10.1007/BF00550087
32. Köferstein R, Jäger L, Zenkner M, Abicht H-P (2008) J Mater Sci 43:832. doi:10.1007/s10853-007-2195-4
33. Köferstein R, Jäger L, Zenkner M, Ebbinghaus SG (2009) J Eur Ceram Soc 29:2317
34. Orlov AV, Shlyakhtin OA, Vinokurov AL, Knotko AV, Tretyakov YD (2005) Inorg Mater 41:1194
35. Muthurajan H, Koteswara Rao N, Gupta UN, Pradhan S, Jha RK, Kumar HH, Mirji SA, Ravi V (2008) Mater Res Bull 43:1842
36. Amsif M, Marrero-López D, Magrasó A, Pena-Martínez J, Ruiz-Morales JC, Núnez P (2009) J Eur Ceram Soc 29:131
37. Xu C, Zhu J, Yang X, Lu L, Wang X (2008) J Rare Earths 26:51
38. Cai J, Laubernds K, Galasso FS, Suib SL, Liu J, Shen X-F, Begge E, Kunz HR, Fenton JM (2005) J Am Ceram Soc 88:2729
39. Almeida de Oliveira AP, Hafsaoui J, Hochepied JF, Berger M-H, Thorel A (2007) J Eur Ceram Soc 27:3597
40. Lin H-L, Chiang RK, Kuo C-L, Chang C-W (2007) J Non-Cryst Solids 353:1188
41. Lee DW, Won JH, Shim KB (2003) Mater Lett 57:3346
42. Su XT, Yan Q-Z, Ma X-H, Zhang W-F, Ge C-C (2006) Solid State Ionics 177:1041
43. Cernea M, Monnereau O, Llewellyn P, Tortet L, Galassi C (2006) J Eur Ceram Soc 26:3241
44. Program WinXPOW v1.06 (1999) Stoe & Cie GmbH, Darmstadt
45. Werner P-E, Eriksson L, Westdahl M (1985) J Appl Cryst 18:367
46. Allred VD, Buxton SR, McBride JP (1957) J Phys Chem 61:117
47. Pfaff G, Hildebrand VD, Fuess H (1998) J Mater Sci Lett 17:1983
48. Dalal PV, Saraf KB (2006) Bull Mater Sci 29:421
49. Subba Rao VV, Rao RVG, Biswas AB (1964) J Am Ceram Soc 47:356
50. Pook N-P, Adam A (2008) Cryst Res Technol 43:1197
51. Griffith P (1964) J Chem Soc 5248–5253
52. Chaudhuri MK, Das B (1986) Inorg Chem 25:168
53. Nakamoto K (1978) Infrared and Raman spectra of inorganic and coordination compounds. Wiley, USA, pp 297
54. Pavlovic VP, Stojanovic BD, Pavlovic VB, Marinkovic-Stanojevic Z, Živković L, Ristic MM (2008) Sci Sinter 40:21
55. Gallagher PK (1965) Inorg Chem 4:965
56. Bera J, Sarkar D (2003) J Electroceram 11:131
57. Chen EL, Sorensen OT, Meng GY, Peng DK (1997) J Thermal Anal 49:1255
58. Earnest CM (1989) Thermochim Acta 137:356
59. PDF 2 (International Centre for Diffraction Data, Pennsylvania) 2001, $BaCeO_3$ [82-2425], $BaCO_3$ [5-378], CeO_2 [75-76], Ba_2GeO_4 [39-127]
60. Buscaglia MT, Bassoli M, Buscaglia V, Alessio R (2005) J Am Ceram Soc 88:2374
61. Köferstein R, Jäger L, Zenkner M, Müller T, Ebbinghaus SG (2010) J Eur Ceram Soc 30:1419
62. Schatt W (1992) Sintervorgänge. VDI-Verlag, Düsseldorf, p 78
63. Knight KS, Bonanos N (1995) Mater Res Bull 30:347
64. Marks GW, Monson LA (1955) Ind Eng Chem 47:1611
65. Novikov II, Portnoj VK (1984) Superplastizität von Legierungen. Deutscher Verlag für Grundstoffindustrie, Leipzig, p.12 et seqq
66. YaE Geguzin, YuI Klinchuk (1976) Poroshkovaya Metallurgiya 7:17
67. Köferstein R, Jäger L, Zenkner M, Müller T, Abicht H-P (2008) Mater Chem Phys 112:531
68. Ohzeki T, Hasegawa S, Shimizu M, Hashimoto T (2009) Solid State Ionics 180:1034
69. Egorov VM, Baikov YuM, Kartenko NF, Melekh BT, Filin YuN (1998) Phys Solid State 40:1911